Argon Cluster Sputtering of a Hybrid Metal–Organic Surface: A Microscopic View

ARTICLE *in* THE JOURNAL OF PHYSICAL CHEMISTRY C · DECEMBER 2012

Impact Factor: 4.77 · DOI: 10.1021/jp3110503

2 AUTHORS:

Oscar A. Restrepo
Université de Montréal
20 PUBLICATIONS **85** CITATIONS
SEE PROFILE

Arnaud Delcorte
Université catholique de Louvain
159 PUBLICATIONS **2,025** CITATIONS
SEE PROFILE

THE JOURNAL OF PHYSICAL CHEMISTRY C

Article

pubs.acs.org/JPCC

Argon Cluster Sputtering of a Hybrid Metal–Organic Surface: A Microscopic View

Oscar A. Restrepo* and Arnaud Delcorte

Institute of Condensed Matter and Nanosciences - Bio & Soft Matter, Université catholique de Louvain, Croix du Sud, 1 bte L7.04.01, B-1348 Louvain-la-Neuve, Belgium

Supporting Information

ABSTRACT: Argon clusters are increasingly used for organic mass spectrometry and 3D imaging, but their interaction with complex samples is not well understood yet. In this study, the interaction of kiloelectronvolt argon cluster projectiles ($Ar_{60-2000}$) with an organic crystal of polyethylene (PE) covered with gold nanoparticles (Au-NPs) is investigated by means of molecular dynamics simulations. The results are compared as a function of the impact point and also to previous simulations involving C_{60} and Au_{400} projectiles. According to the impact point, fragmentation of the polymer or the NP increases monotonically with the energy per atom in the projectile; i.e., the emission of fragments decreases monotonically with increasing cluster size at a given total energy. For impacts on the Au-NP, however, the sputtering yield of organic material exhibits a nonmonotonic dependence on the Ar cluster size, with a maximum for similar projectile and Au-NP sizes. At constant energy per atom, the emission of gold is additionally influenced by the projectile size because larger Ar_n clusters tend to block the emission of Au atoms and clusters. The movies of the simulations also indicate that normal impacts of large clusters such as Ar_{2000} tend to bury large chunks of the Au-NP in the soft matrix, which should be an issue for depth profiling such materials. In the case of finite-size chains, the simulations suggest that emission of large molecules and intact Au-NPs by large Ar_{2000} clusters is possible, even with energies per atom lower than the cohesive energy of the chains, provided that the projectile incidence is oblique (45°).

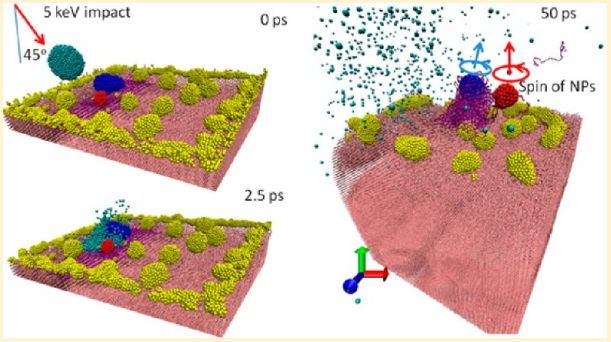

1. INTRODUCTION

Charged clusters, such as SF_5^+, C_{60}^+, Ar_n^+, Au_n^+, and Bi_n^+, constitute the projectiles of choice for the analysis of organic materials by secondary ion mass spectrometry (SIMS). In comparison with atomic beams, they offer a drastic improvement of the sputtering yields and a reduction of the induced damage, which make possible the molecular depth profiling and the 3D analysis of organic solids.[1,2] For depth profiling, SF_5 and C_{60} fail in the analysis of cross-linkable polymers[3] and fullerene-based organic electronics materials.[4] In the case of C_{60}, this is due to the large quantity of bond scissions induced in the sample and to the chemical reactivity of the C atoms distributed in the solid by the projectile, as is explained by recent molecular dynamics (MD) simulations.[5,6] Upon continuous bombardment, cross-linking and dehydrogenation eventually result in the formation of an amorphous carbon surface and in the complete loss of the molecular signal.[7] On the other hand, large metal clusters such as Au_{400}^+, with several hundreds of kiloelectronvolts of energy, have been successfully used to produce molecular ions from some materials, with seemingly excellent surface sensitivity and large molecular ion yields.[8,9] However, it has been shown by simulations that these heavy clusters implant deeper into the soft organic materials, which constitutes a serious issue for depth profiling.[10] Recently, with Ar superclusters, the utopia of a universal projectile that would be adequate for the analysis and depth profiling of all organic samples might have become reality.[2] Large Ar clusters are generally successful in these situations where other clusters fail. Nevertheless, the cluster size, initial energy, angle of impact, and materials leading to the best performance must be better defined and understood. In addition, the efficiency of Ar clusters with inorganic materials remains questionable. A fundamental study involving hybrid samples or composites with metal nanoparticles should therefore help to clarify the behavior of large Ar clusters in these situations.

In the past decade, the sputtering induced by large Ar clusters has been studied both theoretically and experimentally. In particular, MD simulations have been used to investigate the sputtering of several surfaces under different bombardment conditions with Ar_n clusters.[11−14] Properties like surface erosion, depth profiling, and sputtering efficiency using Ar_n clusters are explained in those studies. For instance, the authors have predicted the effect of the impact angle of Ar_{366} and Ar_{2953} projectiles on the efficiency of molecular ejection from a

Received: November 8, 2012
Revised: December 14, 2012

   dx.doi.org/10.1021/jp3110503 | J. Phys. Chem. C XXXX, XXX, XXX−XXX

benzene crystal. The angular dependence of the sputtering yield is strongly affected by the projectile size, with a maximum sputtering yield between 40° and 50° for Ar_{2953} and a plateau for Ar_{366}.[12] For polystyrene on Ag,[13] bulk polystyrene,[6] and arachidic acid multilayers,[15] a threshold energy per atom has been identified, below which fragmentation is minimal. For Ag surfaces, surface roughness also played an important role in the total sputtering yield, and it was influenced by the kinetic energy and the impact angle of the Ar_n cluster.[16] Similar simulations were also conducted with Au_3 and C_{60} projectiles.[14] MD simulations using Ar_n clusters have also been performed to study other materials, e.g., Si, Ni, and other covalent and metallic solids.[17−20] However, the behavior of large molecular systems, such as polymers, upon large Ar cluster impact still needs to be investigated.

Experimentally, the incidence of argon clusters at low energy per atom (∼1 eV)[21] and at angles close to normal[22] favors the emission of intact molecular ions, in contrast to the fragmentation of the organic molecules. Moreover, keeping the energy per atom in the range of the bond dissociation energy allows a control of the broken bond number.[23] At a given acceleration energy, depending on the number of atoms in the projectile, Ar_n clusters can keep the chemical structure intact or seriously damage the target.[24] In a recent article,[25] the Ar_n clusters are studied under two hypotheses: first, the damage accumulation during organic depth profiling should be reduced to a level below that observed with C_{60}; second, the spectra should be "cleaner", i.e., fragmentation should be reduced, and molecular ions at higher mass should be more readily detected. It is indeed concluded that upon 45° incidence, large argon clusters cause less damage accumulation compared to C_{60}, with an approximately constant sputter rate as a function of the Ar cluster size, and that they induce a more gentle ejection in some samples. However, the same study also shows a reduction of the ionization of secondary fragments as the size of the argon cluster increases.

It is known from experiments that Au-NP covered organic surfaces lead to increased emission of characteristic fragments and molecules under atomic Ar^+, Ga^+, and In^+ bombardment, but not with light element clusters such as C_{60}^+.[26−28] The observations have been partly explained using MD simulations.[29] However, to our knowledge, there are no reports in the literature on the behavior of Ar_n clusters with hybrid samples of metal nanoparticles in an organic matrix. Therefore, in this study, we use a system composed of Au-NPs physisorbed on a polyethylene crystal to investigate the projectile energy and size dependence of the sputtering of both the polymer and the metal particles by large Ar clusters. The goal is threefold: (i) compare the emission of polymer and metal upon Ar_n bombardment under different initial conditions; (ii) understand the effect of the metal on the polymer emission in the case of impacts on the Au-NPs; (iii) provide useful indications to improve the experiments. In the process, the physics of the Ar_n cluster−Au-NP impacts is investigated in detail.

2. COMPUTATIONAL METHOD

The construction of the sample with gold NPs has been discussed in previous articles,[10,30] and the detailed explanation of the MD simulation methodology can be found elsewhere.[31,32] In summary, the sample consists of an orthorhombic crystalline structure with 5200 zigzag chains, formed of 200 individual CH_2 coarse grain elements and with dimensions of 300 × 300 × 250 $Å^3$, which gives a density of 0.647 amu/$Å^3$ ≈ 1.07 g/cm^3. The direction of polymerization is parallel to the impact surface. The surface is coated with 13 386 Au atoms forming clusters with 20−30 Å of diameter. Therefore, the total system has 1 053 386 elements.

The interaction potentials implemented in the simulation were the MD/MC-CEM potential for Au−Au,[33] Lennard-Jones potential functions for Au−PE and PE−PE intermolecular interactions, the AIREBO potential for the C−C interactions of the C_{60} projectile,[34] and Morse potential functions for the intramolecular interactions in PE. Additional details about the potential parameters can be found in ref 35. The Ar−Ar and Ar−Au interactions are pair potentials of the LJ form (with ε_{ArAr} = 10.3 meV, r_e = 3.82 Å and ε_{ArAu} = 4.2 meV, r_e = 3.56 Å),[36,37] splined to the repulsive KrC potential valid for close encounters.[38] The Ar−PE interactions were handled with the pure KrC potential because hydrocarbons do not react with Ar atoms. For visualization the VMD program was used.[39]

The sample was introduced into two different reservoirs (Figure 1), with different borders conditions. The first reservoir

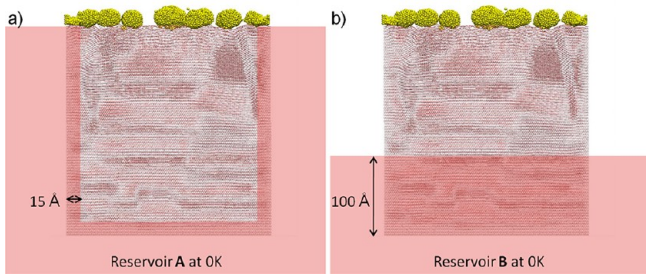

Figure 1. Side views of the sample cells showing the different border conditions and reservoirs used in the simulations.

A was implemented with rigid boundaries of 5 Å and stochastic forces at 0 K over a region of 15 Å, over all the sample sides except the bombarded one. The Langevin equation in the stochastic region provided a heat bath during relaxation and allowed the system to absorb the pressure waves generated by the projectile impact during the bombardment. Thus, in this manner a sample with infinite chains was represented. The second reservoir B was one in which the system was partially immersed in a heat bath, so that the system represented a protuberance over the surface. This reservoir was created by giving stochastic conditions to the atoms from the bottom up to a certain height (Figure 1). The other two sides were kept as before, but the stochastic zone in the bottom was increased from 15 Å to 70 and 100 Å.

The Au-NP-covered polymer was systematically bombarded with Ar cluster projectiles of different sizes (Ar_n, n: 60−2000) and energies (5−20 keV) using the reservoir of Figure 1a. In order to match the values of energy per Ar atom for different cluster sizes, an additional series of simulations were performed with higher energies for the largest clusters (up to 100 eV/atom). All these simulations ran up to 30 ps, and a total of 52 trajectories were computed. Because of the computational expense, only one trajectory was calculated per energy value. With the heat bath B of Figure 1b, 5 and 10 keV impacts were simulated, either with normal (up to 80 ps) and 45° incidence (up to 100 ps). In the latter case, the integration time was increased to better analyze the effects of the rotational motion of the Au-NPs.

dx.doi.org/10.1021/jp3110503 | J. Phys. Chem. C XXXX, XXX, XXX−XXX

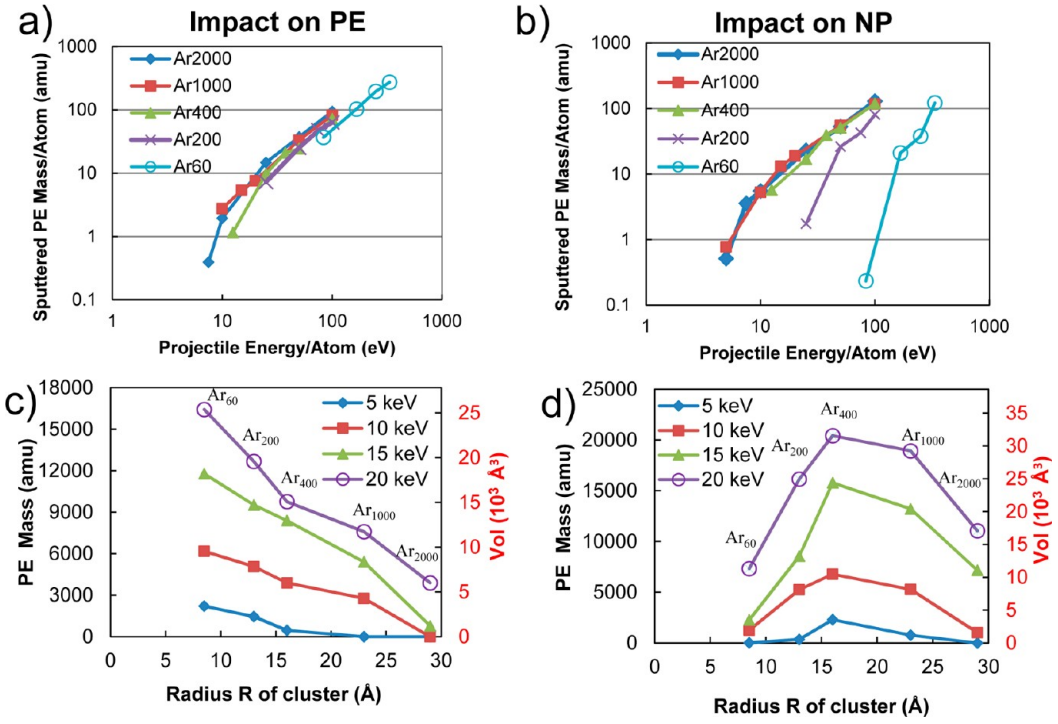

Figure 2. Top: PE sputtered mass per projectile atom as a function of the projectile energy per atom for impacts on (a) the PE and (b) the Au_{555}-NP. Bottom: PE sputtered mass (left) and volume (right) as a function of the radius R of the projectile for impacts on (c) the PE and (d) the Au_{555}-NP.

3. RESULTS AND DISCUSSION

3.1. Effects of the Cluster Size and Energy on Sputtering. The results of PE emission induced by Ar_n clusters are plotted in Figure 2. The figure is divided in two columns: impacts on PE (left) and on the Au-NP (right). In Figure 2a,b, the sputtered mass per Ar atom is plotted as a function of the energy per atom in the projectile. In other words, the sputtering data are scaled to the number of atoms of the respective projectiles. For impacts on PE (Figure 2a), the lines corresponding to the different Ar_n cluster approximately merge on a single, universal line. Above a certain threshold energy, a similar behavior has also been predicted for organic cluster projectiles impinging on amorphous PE[40] as well as other systems.[41−43] The situation is different for impacts on the Au-NP. In that case, the results do not fit in the same line any longer (see in Figure 2b). Only the plots of the larger Ar_n clusters (Ar_{400} and beyond) follow a common trend. The small ones (Ar_{60} and Ar_{200}) show a distinct behavior. From Ar_{400} to Ar_{60}, the efficiency of PE sputtering per Ar atom decreases. Moreover, the slope of the line increases as the number of Ar atoms decreases, indicating a nonlinear evolution of the sputtered PE mass for the smallest clusters. For clusters larger than Ar_{200}, the sputtered PE mass is not strongly influenced by the impact point anymore (PE or Au-NP). Figure 2c,d presents the plots of the total yield of PE for four values of the energy, this time as a function of the radius R of the Ar_n projectiles. As expected from Figure 2a,b, the sputtered mass increases monotonically with energy. In addition, Figure 2c reveals that the total sputtered mass follows a monotonic decrease with increasing projectile radius at all the considered energies when impacts are on PE. Experimentally, a decrease of the sputtering yield with increasing projectile size has been reported for inorganic targets (Au, Si)[44] and for Irganox 1010.[45] In contrast, when the impacts are on the Au-NP (Figure 2d), a maximum sputtered mass of PE is predicted for Ar_{400}.

The snapshots of the trajectory movies corresponding to 20 keV impacts with Ar_{60}, Ar_{400}, and Ar_{2000} (Figure 3) help us to understand the behaviors reported in Figure 2. Trajectories are separated as a function of the aiming point, with impacts on PE in the top rows and impacts on the Au-NP in the bottom rows. For impacts on PE, the initial crater width increases with increasing projectile radius, but the number of broken bonds decreases because of the decreasing energy per atom in the cluster as indicated by the reduction of the number of sputtered fragments (Figure 2). In addition, the snapshots taken at 5 ps show that the larger Ar clusters block the emission of the polymer fragments because of the high density of Ar atoms that remain in the forming crater and above it. This combination of factors explains the behavior of Figure 2c. For impacts on the Au-NP, a strong backscattering of Ar_{60} is accompanied by the Au-NP fragmentation (similar to Ar_{200}, not shown). About ~20% of the Ar_{60} energy is reflected with the scattered atoms into the vacuum at 20 keV, and it goes up to ~30% at 5 keV. On the other hand, the projectiles that are larger than Ar_{400} tend to cover the Au-NP, reducing its fragmentation. The situation is clearly illustrated with the case of Ar_{2000}, which splashes over the surface and pushes the squished Au-NP into the polymer at 5 ps. The maximum sputtered mass for Ar_{400} in Figure 2d can therefore be rationalized considering the fact that Ar_{400} is the cluster that has the closest radius to the targeted Au-NP (the radius of the Au_{555} target NP is $R_{NP} \sim 14$ Å, while for Ar_{400} it is $R \sim 16$ Å). For $R < R_{NP}$, all the Ar atoms of the projectile collide with Au atoms that are 5 times heavier, and as a result, they are essentially backscattered into the vacuum. On the other hand, for $R > R_{NP}$, those Ar atoms that are beyond of R_{NP} continue their trajectory until they are stopped (and not strongly reflected) by PE atoms which are 3 times lighter. From

dx.doi.org/10.1021/jp3110503 | J. Phys. Chem. C XXXX, XXX, XXX−XXX

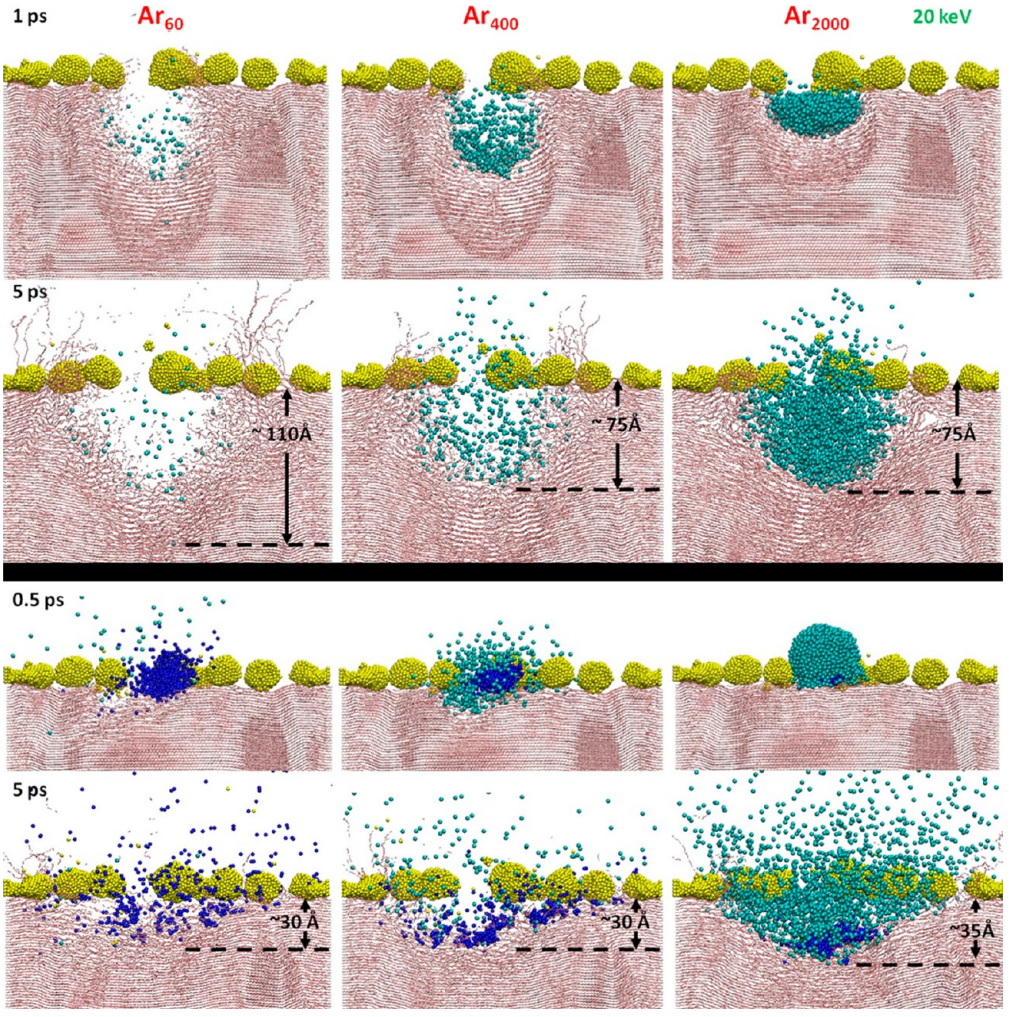

Figure 3. 20 keV Ar_{60}, Ar_{400}, and Ar_{2000} projectile impacts. Top panel: impacts over PE. Bottom panel: impacts on the central Au-NP. The respective maximum implantation depths are shown at 5 ps. Color code: pink is PE, cyan is the projectile, and yellow signifies the Au-NPs. The target Au_{555}-NP is in dark blue.

Ar_{60} to Ar_{400}, an increasing number of Ar atoms with a substantial initial kinetic energy (larger than 50 eV in any case) are deflected toward the polymer surface. Together with Au-NP fragments, they break bonds in the organic solid and, eventually, induce the emission of polymer fragments. Beyond Ar_{400}, Figure 2 also shows that impacts on the Au-NP are consistently >2 times more efficient at sputtering organic material than impacts on the polymer. Our interpretation, supported by the movies of the simulations, is that the Au-NP helps redirecting the Ar atoms laterally, causing bond breaking and the possibility of fragment emission at larger distances of the impact point, where the blocking effect of the Ar cloud is less important. This effect is illustrated in Figure 3 by the wider distribution of Ar atoms at 5 ps for Ar_{2000} impacts on the Au-NP.

For a better understanding of the Au-NP fragmentation upon direct impact, Figure 4 shows the sputtered Au atom mass as a function of the energy of the Ar_n cluster scaled by the number of atoms in the projectile. In this graph, clusters of Au atoms, including larger fragments from the central Au-NP or other intact Au-NPs desorbed from other locations on the surface, are not taken into account. These represent a very large fraction of the sputtered mass in some cases, but consistently less than 10% of the ejected gold particle numbers. Our results show

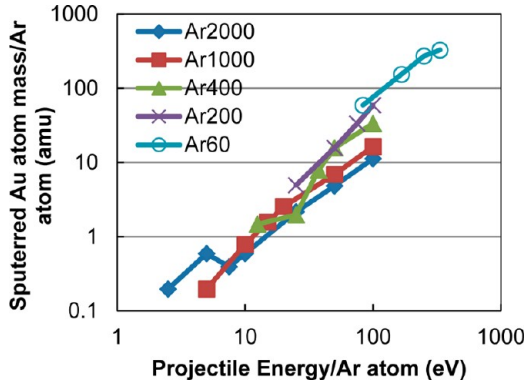

Figure 4. Energy dependence of the sputtered mass of Au atoms (only monomers), scaled by the number of atoms in the projectile. Impacts are on the central Au_{555}-NP.

that, unlike the number of sputtered Au atoms, the total sputtered Au mass exhibits large fluctuations, probably because of the nature of the target (not shown). The trajectory movies and Figure 3 indicate that, under impact, the nanoparticle may fragment in many ways, and because of its finite size and its round shape, large clusters of atoms can detach and move in any direction, being either sputtered or ending up in the

dx.doi.org/10.1021/jp3110503 | J. Phys. Chem. C XXXX, XXX, XXX−XXX

surface. Depending on their fate, such large clusters will be counted as sputtered or not, strongly affecting the calculated sputtered mass. Considering only single Au atoms, which are sputtered in large numbers, alleviates this problem. Because single Au atoms represent the largest part of the sputtered flux, the trends of Figure 4 also provide a good image of the extent of the Au-NP fragmentation. As it was the case for sputtered PE (see Figure 2a for comparison), the emission of Au atoms and the fragmentation increase with the energy per atom in the Ar cluster. However, in comparison with the impacts on PE, the scaling by the number of atoms reveals another effect. At high energy, large Ar_n clusters produce less sputtered fragments than smaller clusters for the same energy per atom. For instance, at 100 eV per atom, a reduction by a factor of 5 is observed. This can be explained by the fact that Ar_{2000} completely covers the cluster, restricting the movement of the gold atoms. This effect is corroborated in Figure 3 by the movie snapshots at 5 ps, showing that the Au fragment size (blue) increases with the projectile size.

3.2. Ar_n versus Other Cluster Projectiles. As is shown in Figure 2, Ar_{60} exhibits extreme properties in terms of sputtering, with the lowest sputtered PE yield when the impact is on the Au-NP and the highest yield when the impact is over the PE. In Table 1, the sputtering performance of 10 keV Ar_{60} is compared with that of isoenergetic C_{60}, which has the same number of atoms but a lower atomic mass.[29] Because of the important fluctuations discussed earlier in terms of sputtered mass, it is difficult to compare the emission of Au for these different projectiles. Therefore, we restrict our analysis to the emission of PE fragments.

Table 1. Comparison of the Total Sputtered PE Fragment Numbers and Masses for 10 keV Ar_{60} and C_{60} Bombardment

	on PE		on Au-NP	
	fragments	mass (kDa)	fragments	mass (kDa)
Ar_{60}	229	6.174	19	1.260
C_{60}	313	8.456	15	0.476

For impacts on the polymer, the PE sputtering yield (defined as the number of sputtered fragments per projectile) is 1/3 less for Ar_{60} than for C_{60}. This difference is rather small given the 3 times larger atomic mass of Ar. However, one must take into account that Ar_{60}, being a van der Waals cluster, has much less cohesive energy than C_{60}. The microscopic analysis of the event shows that, for this reason, Ar_{60} spreads in an approximately spherical region of the PE surface upon impact. C_{60} behaves the same, but for another reason, that is because its atomic mass matches the atomic mass of the organic target, leading to maximum energy transfer and deflection in diatomic collisions. When the impact is on the Au-NP, Ar_{60} shows better performance in transferring its energy to the system because the atomic mass ratio between the projectile and the metal target is closer to one. The increase in fragment numbers is rather small, but the sputtered mass is 2−3 times larger.

In recent experimental studies, Au_{400} has been proposed as a promising projectile for the analysis of materials.[8] In Table 2, the sputtering induced by Au_{400} is compared with that of Ar_{400} (same number of atoms) and of Ar_{2000} (same mass). The energy of the clusters is 20 keV. Irrespective of the impact point, Ar_{400} induces the highest sputtering yields of PE. The numbers of fragments and the masses of PE emitted by Au_{400} are closer to those calculated for Ar_{2000}, though they are smaller, especially for the impacts on PE. The analysis of the trajectories indicates that Au_{400} with its large momentum per projected surface area[46] and cohesive energy penetrates deep in the polymer without diverging,[10] causing comparatively small perturbation of the surface and sputtering at normal incidence. For impacts on the Au-NP, the large mass and cohesive energy of the Au_{400} cluster play in the same manner but the difference is reduced, because, on one hand, the stopping of the Au_{400} in the surface is much more efficient and, on the other hand, a significant part of the lighter Ar_n cluster energy is backscattered in the vacuum with the atoms of the projectile.

Table 2. Comparison of the Total Number of Sputtered PE Fragments and Masses for 20 keV Au_{400}, Ar_{400}, and Ar_{2000} Bombardment

	on PE		on Au-NP	
	fragments	mass (kDa)	fragments	mass (kDa)
Au_{400}	15	0.756	99	7.602
Ar_{400}	283	9.758	457	20.426
Ar_{2000}	21	3.892	146	11.046

3.3. Detailed Analysis of Low-Energy Ar_{2000} Impacts. The sputtering results shown in Figure 2 suggest that Ar_n clusters with less than 10 eV of energy per atom, i.e., with an energy close to the covalent bond energy in the chains, induce minimal fragmentation in the organic sample. As mentioned in the Introduction, this is in agreement with experiments and previous simulations involving either carbon-based cluster projectiles bombarding bulk organic samples[40] or Ar projectiles impinging on molecular overlayers.[13] This energy range is therefore of special interest for the emission of unfragmented large organic molecules and damageless molecular depth profiling. In order to have a more complete view of the interaction of such low-energy projectiles with our hybrid metal−organic target, a series of simulations were run without rigid borders in the top part of the sample (see the Computational Method section), so that the flat-lying chains now mimic oligomers with a finite length, rather than infinite chains. In that slightly modified configuration, the surface layer is constituted of free oligomers of 2.8 kDa each. The goal of these new simulations is twofold: (i) to compare the case of kDa oligomer bombardment with that of polymers with "infinite" chain length in these limit conditions; (ii) to study the ability of relatively low energy Ar cluster to desorb intact PE molecules or large PE fragments and metal NPs.

As an illustration, perspective and side views of the 5 keV impact of Ar_{2000}, with normal incidence, on the metal organic sample with free border conditions, are shown in the top part of Figure 5. Despite the free borders, the emission of intact PE chains or entire Au-NPs was not observed, even after a time of 80 ps. Instead, the chains move to the sides and tend to wrap around the Au-NPs. With respect to the sample in which chains ends were tied to the borders, this sample with free border conditions shows a more severe plastic deformation. Much of the energy is dissipated in internal energy rather than used to produce molecular emission. The plasticity of soft organic materials can therefore be considered as a drawback for the sputtering of large molecules when the impact angle is normal to the surface. Another reason why intact PE oligomers are not ejected is because they are very long, linear, and bonded to the crystal over their entire length. Previous simulations using shorter, flat-lying, hexacontane molecules indicated that those

dx.doi.org/10.1021/jp3110503 | J. Phys. Chem. C XXXX, XXX, XXX−XXX

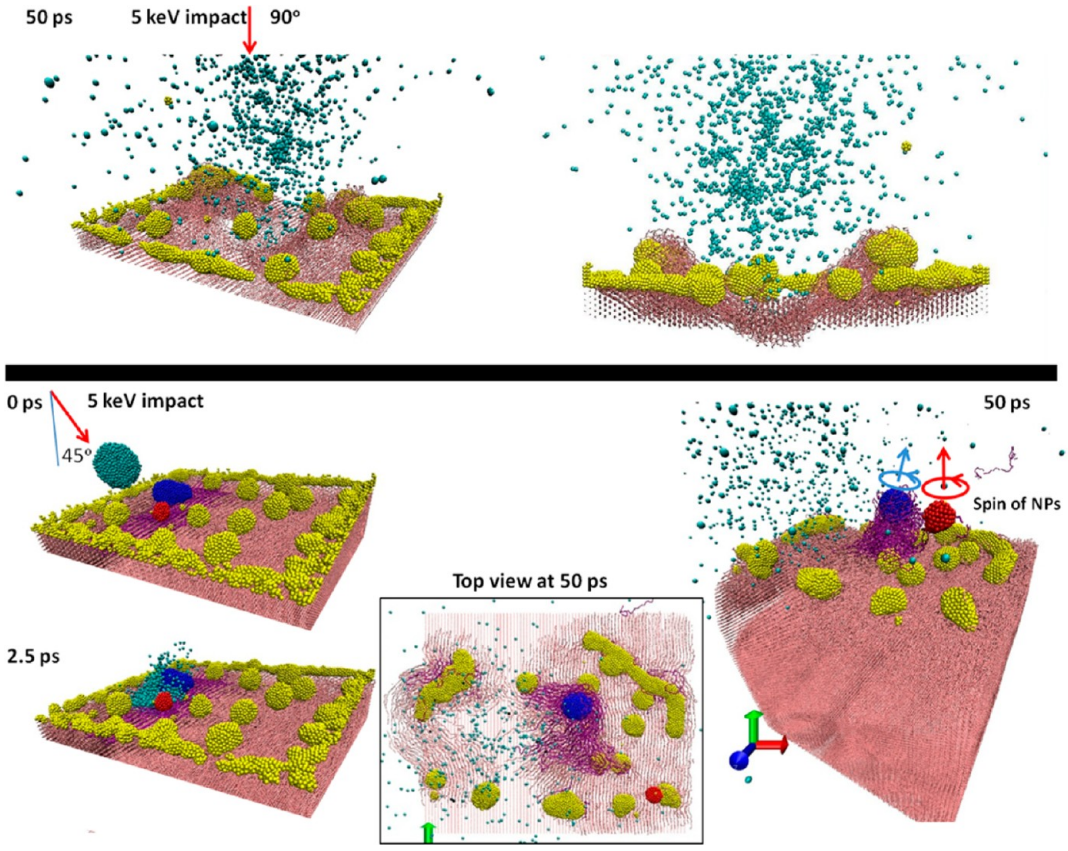

Figure 5. 5 keV Ar_{2000} impacts with an incidence of 0° (top panel) and 45° (bottom panel). The color scheme is essentially the same as Figure 3, except for the target Au-NPs: Au_{217} is colored in red and Au_{1194} in blue. Purple represents the PE chains that protrude as a consequence of the rotational motion of the Au-NPs.

were relatively easily sputtered by 5−10 keV cluster projectiles.[35]

On the other hand, if the impact angle with respect to the surface is changed from normal to oblique, the emission of large PE molecules and Au-NPs becomes possible, as shown in the bottom part of Figure 5 for a 5 keV Ar_{2000} impact, with 45° incidence and an azimuth perpendicular to the direction of the polymer chains. The snapshots of the simulations show that, upon impact, molecules of PE wrap around the Au-NPs which move upward with a rotational motion. In the process, one Au-NP (Au_{217} in red) and one molecule are ejected, while the other Au-NP (Au_{1194} in blue) remains attached to the surface via a group of entangled molecules. This mechanism clearly differs from the normal impacts. In particular, the rotational motion of the Au-NPs could lead to the emission metal−organic adducts. Indeed, the rotational motion, combined with the large surface energy of the metal NP surface, favors the association of the PE chains with the Au-NPs. The total kinetic energy, K, and the kinetic energy of the center of mass, K_{cm}, of the two Au-NPs directly impacted by the projectile, Au_{217} and Au_{1194}, are given in Figure 6. In both plots, K shows typical fluctuations due to the interchange of the kinetic and potential energies, while the smoother curve of K_{cm} is only perturbed by the interaction with the external forces, i.e., the interactions with the PE chains. The Au_{217} NP interacts with the polymer chains only during the first 40 ps. After that, it moves into the vacuum as a free particle, as indicated by the flat kinetic energy profile. The difference between the two curves, i.e., the relative kinetic energy, indicates a maximum excitation of 0.14 eV/Au atom. The maximum relative kinetic energy gained by the

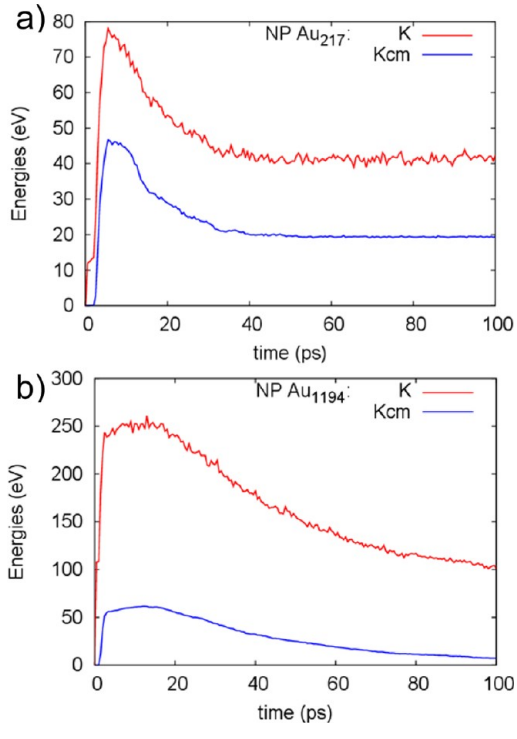

Figure 6. Time evolution of the total kinetic energy (K) and the center-of-mass kinetic energy (K_{cm}) of the Au-NPs considered in Figure 5, Au_{217} and Au_{1194}.

dx.doi.org/10.1021/jp3110503 | J. Phys. Chem. C XXXX, XXX, XXX−XXX

Au_{1194} NP is slightly larger, 0.17 eV/Au atom, but the fraction of the projectile energy transferred in translational motion is much lower. Because of the strong interaction with the polymer chains, the Au_{1194} NP slows down, and after 100 ps, it is almost completely still. At the end of the trajectory, it has also significantly cooled, and its relative kinetic energy is under 0.1 eV/Au atom.

This mechanistic study shows that metal NPs and kilodalton molecules can be emitted by low-energy Ar_{2000} clusters, in an energy regime where fragmentation is minimal (<10 eV/Ar atom). In agreement with previous results involving large organic projectiles impinging on a polymeric sample, the emission of large polyatomic species appears to be favored by the oblique incidence of the projectile and the emission is strongly forward-directed.[47]

4. CONCLUSION

The sputtering behavior of a high-molecular-weight polyethylene crystal ("infinite" chains) with supported metal nanoparticles was explored using MD simulations. Upon small Ar cluster bombardment (Ar_{60-200}), the PE sputtered mass strongly depends on whether the impacts are on the polymer or on the NPs. The difference is reduced for Ar clusters that are larger than the NPs. In the case of impacts on the PE, the sputtering yield follows a universal line as a function of the energy per atom for all the projectiles, meaning that this parameter governs the polymer fragmentation. For a given total energy, the sputtering yield decreases with increasing cluster size. However, the situation is different when the impacts are on the Au-NP. In that case, for all the tested impact energies, the sputtered PE mass follows a nonmonotonic evolution as a function of the Ar cluster size, with a maximum when the size of the projectile and the Au-NP match. Even though the fluctuations of Au sputtered mass are important, our analysis indicates that the energy per atom in the projectile is also the main parameter explaining the fragmentation of the Au-NP. The movies of the simulations indicate that normal impacts of large clusters such as Ar_{2000} tend to bury large chunks of the Au-NP in the soft matrix. Smaller clusters should therefore be more appropriate for depth profiling such hybrid materials.

On the other hand, the analysis of 5 keV Ar_{2000} impacts under different boundary conditions shows that the emission of flat-lying kilodalton molecules and Au-NPs is difficult at normal incidence, due to the high plasticity of the PE, which absorbs much of the energy through deformation. However, the ejection of both molecules and Au-NPs is observed at 45° incidence angle, via a washing mechanism. Rotational motion of the Au-NPs helps the emission of large PE chains.

From the analytical point of view, because Ar_n projectiles stop in the very surface of the solid, they can be considered as equally suited as C_{60} for surface characterization and the sputtered PE masses of isoenergetic Ar_{60} and C_{60} are comparable.

■ ASSOCIATED CONTENT

Supporting Information

A video of Ar_{2000} 5 keV impact at 45°. This material is available free of charge via the Internet at http://pubs.acs.org.

■ AUTHOR INFORMATION

Corresponding Author

*E-mail oscar.restrepo@uclouvain.be.

Notes

The authors declare no competing financial interest.

■ ACKNOWLEDGMENTS

The authors thank Professor Barbara J. Garrison from Penn State University for the access to her simulation code for MD simulations. This work and O.A.R. are supported by the French Community of Belgium via the Concerted Research Action programme (ARC NANHYMO: convention 07/12-003) and by the European Community under the FP7 project 3D-Nanochemiscope (Grant agreement: CP-TP 200613-2). A.D. is a Senior Research Associate of the Belgian Fonds National pour la Recherche Scientifique (FNRS). Computational resources have been provided by the supercomputing facilities of the Université catholique de Louvain (CISM/UCL).

■ REFERENCES

(1) Winograd, N. *Anal. Chem.* **2005**, *77*, 143−149.
(2) Lee, J. L. S.; Ninomiya, S.; Matsuo, J.; Gilmore, I. S.; Seah, M. P.; Shard, A. G. *Anal. Chem.* **2010**, *82*, 98−105.
(3) Mahoney, Ch. *Mass Spectrom. Rev.* **2010**, *29*, 247−293.
(4) Mouhib, T.; Poleunis, C.; Möllers, R.; Niehuis, E.; Defrance, P.; Bertrand, P.; Delcorte, A. *Surf. Interface Anal.* **2012**, DOI: 10.1002/sia.5052.
(5) Webb, R. P.; Garrison, B. J.; Vickerman, J. C. *Surf. Interface Anal.* **2011**, *43*, 116−119.
(6) Czerwinski, B.; Postawa, Z.; Garrison, B. J.; Delcorte, A. *Nucl. Instrum. Meth. Phys. Res. B* http://dx.doi.org/10.1016/j.nimb.2012.11.030.
(7) Shard, A. G.; Green, F. M.; Brewer, P. J.; Seah, M. P.; Gilmore, I. S. *J. Phys. Chem. B* **2008**, *112*, 2596−2605.
(8) Tempez, A.; et al. *Rapid Commun. Mass Spectrom.* **2004**, *18*, 371−376.
(9) Novikov, A.; Caroff, M.; Della-Negra, S.; Depauw, J.; Fallavier, M.; Beyec, Y.; Le; Pautrat, M.; Schultz, J. A.; Tempez, A.; Woods, A. S. *Rapid Commun. Mass Spectrom.* **2005**, *19*, 1851−1857.
(10) Restrepo, O. A.; Delcorte, A. *J. Phys. Chem. C* **2011**, *115*, 12751−12759.
(11) Rzeznik, L.; Czerwinski, B.; Paruch, R.; Garrison, B. J.; Postawa, Z. *Nucl. Instrum. Methods Phys. Res., Sect. B* **2009**, *267*, 1436−1439.
(12) Czerwinski, B.; Rzeznik, L.; Paruch, R.; Garrison, B. J.; Postawa, Z. *Nucl. Instrum. Methods Phys. Res., Sect. B* **2011**, *269*, 1578−1581.
(13) Rzeznik, L.; Czerwinski, B.; Garrison, B. J.; Winograd, N.; Postawa, Z. *J. Phys. Chem. C* **2008**, *112*, 521−531.
(14) Postawa, Z.; Rzeznik, L.; Paruch, R. *Surf. Interface Anal.* **2011**, *43*, 12−15.
(15) Rzeznik, L.; Paruch, R.; Czerwinski, B.; Garrison, B. J.; Postawa, Z. *Vacuum* **2009**, *83*, S155−S158.
(16) Rzeznik, L.; Paruch, R.; Garrison, B. J.; Postawa, Z. *Nucl. Instrum. Methods Phys. Res., Sect. B* **2011**, *269*, 1586−1590.
(17) Aoki, T.; Matsuo, J. *Nucl. Instrum. Methods Phys. Res., Sect. B* **2006**, *242*, 517−519.
(18) Cheng, Y.; Lee, C. *Nucl. Instrum. Methods Phys. Res., Sect. B* **2009**, *267*, 1428−1431.
(19) Samela, J.; Nordlund, K. *Phys. Rev. B* **2010**, *81*, 1−5.
(20) Samela, J.; Nordlund, K.; Keinonen, J. *Eur. Phys. J. D* **2007**, *43*, 181−184.
(21) Ninomiya, S.; Nakata, Y.; Ichiki, K.; Seki, T.; Aoki, T.; Matsuo, J. *Nucl. Instrum. Methods Phys. Res.* **2007**, *256*, 493−496.
(22) Oshima, S.; Kashihara, I.; Moritani, K.; Inui, N.; Mochiji, K. *Rapid Commun. Mass Spectrom.* **2011**, *25*, 1070−1074.
(23) Moritani, K.; Mukai, G.; Hashinokuchi, M.; Mochiji, K. *Appl. Phys. Express* **2009**, *2*, 046001−046003.
(24) Yamamoto, Y.; Ichiki, K.; Ninomiya, S.; Seki, T.; Aoki, T.; Matsuo, J. *AIP Conf. Proc.* **2011**, *1321*, 298.
(25) Rabbani, S.; Barber, A.; Fletcher, J.; Lockyer, N. P.; Vickerman, J. C. *Anal. Chem.* **2011**, *83*, 3793−3800.

(26) Delcorte, A.; Yunus, S.; Wehbe, N.; Nieuwjaer, N.; Poleunis, C.; Felten, A.; Houssiau, L.; Pireaux, J.-J.; Bertrand, P. *Anal. Chem.* **2007**, *79*, 3673−3689.
(27) Heile, A.; Lipinsky, D.; Wehbe, N.; Delcorte, A.; Bertrand, P.; Felten, A.; Houssiau, L.; Pireaux, J.; Demondt, R.; Vanvaeck, L. *Appl. Surf. Sci.* **2008**, *255*, 941−943.
(28) Heile, A.; Muhmann, C.; Lipinsky, D.; Arlinghaus, H. F. *Surf. Interface Anal.* **2011**, *43*, 20−23.
(29) Restrepo, O. A.; Delcorte, A. *Surf. Interface Anal.* **2011**, *43*, 70−73.
(30) Restrepo, O. A.; Prabhakaran, A.; Delcorte, A. *Nucl. Instrum. Methods Phys. Res., Sect. B* **2011**, *269*, 1595−1599.
(31) Garrison, B. J. *Chem. Soc. Rev.* **1992**, *21*, 155−162.
(32) Garrison, B. J. In *ToF-SIMS: Surface Analysis by Mass Spectrometry*; Vickerman, J. C., Briggs, D., Eds.; Surface Spectra: Manchester, UK, 2001; pp 223−257.
(33) Stave, M. S.; Sander, D. E.; Raeker, T. J.; DePristo, A. E. *J. Chem. Phys.* **1990**, *93*, 4413−4426.
(34) Stuart, S. J.; Tutein, A. B.; Harrison, J. A. *J. Chem. Phys.* **2000**, *112*, 6472−6486.
(35) Hamraoui, K.; Delcorte, A. *J. Phys. Chem. C* **2010**, *114*, 5458−5467.
(36) Rappe, A. K.; Casewit, C. J.; Colwell, K. S.; Goddard, W. a.; Skiff, W. M. *J. Am. Chem. Soc.* **1992**, *114*, 10024−10035.
(37) Mayo, S. L.; Olafson, B. D.; Goddard, W. A. *J. Phys. Chem.* **1990**, *94*, 8897−8909.
(38) O'connor, D.; Biersack, J. *Nucl. Instrum. Methods Phys. Res., Sect. B* **1986**, *15*, 14−19.
(39) Humphrey, W.; Dalke, A.; Schulten, K. VMD - Visual Molecular Dynamics. *J. Mol. Graphics* **1996**, *14*, 33−38.
(40) Delcorte, A.; Garrison, B. J.; Hamraoui, K. *Anal. Chem.* **2009**, *81*, 6676−6686.
(41) Anders, C.; Ziegenhain, G.; Zimmermann, S.; Urbassek, H. M. *Nucl. Instrum. Methods Phys. Res., Sect. B* **2009**, *267*, 3122−3125.
(42) Anders, C.; Urbassek, H. M. *Nucl. Instrum. Methods Phys. Res., Sect. B* **2009**, *267*, 3227−3231.
(43) Ryan, K. E.; Garrison, B. J. *Anal. Chem.* **2008**, *80*, 6666−6670.
(44) Seki, T.; Murase, T.; Matsuo, J. *Nucl. Instrum. Methods Phys. Res., Sect. B* **2006**, *242*, 179−181.
(45) Niehuis, E.; Möllers, R.; Rading, D.; Cramer, H.-G.; Kersting, R. *Surf. Interface Anal.* **2012**, DOI: 10.1002/sia.5079.
(46) Popok, V. N.; Vučković, S.; Samela, J.; Järvi, T. T.; Nordlund, K.; Campbell, E. E. B. *Phys. Rev. B* **2009**, *80* (205419), 1−12.
(47) Delcorte, A.; Garrison, B. J. *Nucl. Instrum. Methods Phys. Res., Sect. B* **2011**, *269*, 1572−1577.